Materials Today Communications 26 (2021) 101993

Contents lists available at ScienceDirect

Materials Today Communications

journal homepage: www.elsevier.com/locate/mtcomm

Rapid synthesis of a novel nano-crystalline mesoporous faujasite type metal-organic framework, ZIF-8 catalyst, its detailed characterization, and $NaBH_4$ assisted, enhanced catalytic Rhodamine B degradation

Suman Chirra [a,b], Li-Fang Wang [b], Himanshu Aggarwal [c], Ming-Fong Tsai [b], Siva Sankari Soorian [b], Suresh Siliveri [a], Srinath Goskula [a], Sripal Reddy Gujjula [a], Venkatathri Narayanan [a,*]

[a] Department of Chemistry, National Institute of Technology, Warangal 506 004, Telangana, India
[b] Department of Medicinal & Applied Chemistry, College of Life Science, Kaohsiung Medical University, Kaohsiung 807, Taiwan
[c] Department of Chemistry, Birla Institute of Technology and Science-Pilani, Hyderabad Campus, Jawahar Nagar, Shamirpet, Hyderabad, India

ARTICLE INFO

Keywords:
Metal-organic framework
ZIF-8
Mesoporous
Faujasite type
Rhodamine B degradation

ABSTRACT

In this manuscript, we have reported a strategy for the synthesis and fine control of the crystal size and morphology of a novel mesoporous faujasite type zeolitic imidazolate framework-8 (ZIF-8) nanocrystals in water solution. The synthesized materials are mesoporous faujasite type, highly crystalline, nanometer-sized, and with a high surface area. The materials have been characterized using powder X-ray diffraction (XRD), transmission electron micrograph (TEM), BET-Surface area, and Fourier transform infrared spectroscopic (FT-IR) analysis. The distribution of nanoparticles is observed through DLS spectroscopy. The thermogravimetry/differential thermal analysis reveals that the material is stable even up to 600 °C. Tetrahedral coordination and 4+ oxidation state of Zinc is found through UV–vis and X-ray photoelectron spectroscopies. The $NaBH_4$ assisted rhodamine B degradation at room temperature shows excellent catalytic activity (~ 95 %) in a short duration (10 min.). A plausible mechanism of degradation on its catalytic activity is also proposed.

1. Introduction

Nanomaterials offer desirable properties that are difficult to achieve with bulk materials. Nanomaterials have pervaded all aspects of technology, providing fascinating novel features and enhanced enactment over bulk materials. However, producing uniform sized nanomaterials at a large scale in a green route remains a great dispute. Research in the area of porous materials plays a vital role in research and industry. Nano-sized porous catalyst particles offer a greater external surface area and, for that reason, increased catalytic activity.

Over the earlier two decades, gigantic attention has been paid to the synthesis, properties, and versatile applications of microporous polymeric materials due to their uniform pore size and ease of functional tunability. Metal-organic frameworks (MOFs), also known as inorganic−organic hybrid materials, have come into view as one of the most studied classes of highly crystalline nanoporous solid materials. These are composed of metal ions/clusters coordinated to organic ligands to form three-dimensional (3D) crystalline porous networks. Due to their superior properties like very high surface area, nanometer-sized cavities, regular channels, high stability, chemical tunability, and high crystallinity. MOFs offer many potential opportunities in the fields of gas separation and gas sorption, [1–5] biosensing [6], molecular sensing [7], catalysis [8–10], drug delivery [11–13], chemical separations [14, 15], and energy storage [16]. Zeolitic imidazolate systems (ZIFs) are a subclass of nanoporous MOFs that have structural comparability with zeolites. The ZIFs have preferences over zeolites since the hybrid metal-organic framework structures offer greater adaptability in terms of design, functionality, and surface properties [17,18].

Zeolitic imidazolate frameworks (ZIFs) are a subseries of metal-organic frameworks (MOFs) that have structural similarities with molecular sieves like zeolites. They show excellent thermal stability and chemical stability as well. The synthesis of ZIFs can be carried out under usual conditions like room temperature and by using a simple sol-gel method with good yields. ZIFs are an exciting class of crystalline

* Corresponding author.
E-mail address: venkatathrin@yahoo.com (V. Narayanan).

https://doi.org/10.1016/j.mtcomm.2020.101993
Received 28 May 2020; Received in revised form 25 November 2020; Accepted 18 December 2020
Available online 28 December 2020

microporous materials as they showcase distinctive and highly attractive properties from both zeolites and MOFs, such as a remarkable high surface area with large micropore volume, precise control of the pore size, high crystallinity, uniform micropores, and high thermal and chemical stability. ZIF-8 is of the most extensively studied materials among the ZIFs [19]. ZIF-8 ($Zn(mIM)_2$, where mIM = 2- methyl imidazolate) owns few of these characteristics; the material is stable up to 500 °C and having high internal surface area facilitates excellent sorption properties, which makes this material most exciting and most studied framework in the large ZIF family, containing a cubic lattice (space group I43 m) and a faujasite zeolite topology. The structural topologies of ZIFs are similar to zeolite or zeolite-like topologies. ZIFs usually consist of Zn or Co metal centers, and to this, imidazole-derived organic linkers will be coordinated tetrahedrally. The bond angle of this metal − imidazole − metal bond is very close to that of the Si − O–Si bond angle in zeolites, whose value is usually 145°. Many composite materials of ZIFs have been reported to improve the mechanical strength and other properties for various practical applications, ZIFs with metal oxide, [20] with the surfactant, [21], and also with a polymer [22]. Among all known ZIF materials, ZIF-8 (2- methyl imidazole zinc salt) is acclaimed as an admirable member because of its economic production and has been experimented with widely. Contrasted with different kinds of metal-organic framework materials, ZIFs often indicated better thermal, hydrothermal, and chemical stabilities. Thus, ZIFs have pilled in increasingly more consideration in numerous applications, for example, gas storage, [23] separations [24], catalysis, [25], and chemical sensors [26].

The reactions in aqueous media are of brilliant importance for large-scale industrial developments since water is available in abundance, and it offers a cost-effective approach. However, the toxicity occurring as a result of chemical processes remains a serious complexity for sustaining ecological equilibrium and, more significantly, for environmental entropy of the current as well as future generations. This can be dealt with the help of green chemistry. Green chemistry mainly involves the usage of environmentally friendly solvents, catalysts, ensuing in no wastage of starting materials, and conversion of the ensuing or all the starting materials into the preferred product [27].

To the best of our knowledge, all ZIFs detailed in the literature so far were made in organic solvents, for example, dimethylformamide (DMF), diethyl formamide (DEF), and methanol. Organic solvents are costly and harmful to the environment. Water medium is a great alternative and it has been used in the case of 1D materials, small pore, or non-permeable materials [28]. In the present work, we report the principal case of ZIFs, e.g., hybrid three-dimensional large pore faujasite like mesoporous ZIF-8, synthesized in water. Traditional ZIF-8 has the three-dimensional small pore Sodalite type zeolitic structure. It was accounted for by Yaghi's research group utilizing a solvothermal preparation strategy in DMF [29]. A few ongoing reports investigated the synthesis of ZIF-8 in different solvents, for example, methanol, DMF-methanol, [30], and H_2O-methanol combinations [31] and so on. The synthesis time is typically extended from one hour to one month. Some of these reports are based on nanometer-sized ZIF-8 crystals or control the crystal morphology [32]. These outcomes showed the potential use of ZIF-8 for the enormous scope of modern industrial applications. The technique reported here offers a quick and economic strategy for the synthesis of hybrid faujasite like mesoporous ZIF-8.

Due to the fast increment of the global population, unplanned urbanization, agriculture activities, and rapid development of industries, the water sources have been heavily contaminated with wastes such as organic dyes that pose a severe threat to the ecosystem. The detonated wastewater encompasses chemicals, perhaps dyes distributed into the natural watercourse from industries comprising a tannery, textile, food, paper, pulp, leather, cotton, wood, silk, plastics, cosmetics, and other industries [33–38]. Among these industries, the main component of sewage comes from the textile industries that consume over 700,000 tons of dyes. Dye wastewater so often has the features that are inert and non-biodegradable (low biodegradability), with deep color high chromaticity, and biological oxidation necessities, and high chemical oxygen demand (COD). Because of the oncogenic and mutagenic consequences, the majority of dyes are considered to be very toxic and can cause potential damage to animals and plants, including human health [39].

Various methods such as biological treatment techniques, chemical coagulation, flocculation, ion-exchange, enzymatic oxidation, membrane filtration, adsorption, photocatalysis, chemical oxidation, electrochemical process, aerobic, anaerobic microbial degradation, electrolytic chemical treatment, and advanced oxidation technologies (AOPs) have been investigated for the degradation of dye-polluted wastewaters [40,65]. However, many of these techniques are inadequate in actual application because of their high price, secondary pollution, low efficiency, and slow kinetics. Among the methods as mentioned earlier, adsorption is an essential and attractive technique to eliminate dyes from industrial water contaminants because of its advantages like easy operation process, economic feasibility (less cost), high efficiency, eco-friendly, less energy consumption, and no byproduct or side product formation and also less process time [41–46]. Therefore, the need for better adsorbents with high efficiency is always warranted.

In recent times, the applications of MOFs as an adsorbent has attained substantial attention due to its diversity, porosity, easy tunability, high stability, and high surface area. The ZIFs, a subclass of MOFs, not merely have the benefits of MOFs but also have higher thermal and chemical stability. $NaBH_4$ treated rhodamine B is used as a target organic pollutant to probe its conduct over ZIF-8. Since RhB is a poisonous dye that is harmful to the environment, humans, and animals, RhB wastewater has become a serious concern. It is one of the essential xanthene dyes (triphenylmethane family), which contains four *N*-ethyl groups at either side of the xanthene ring, commonly used in the textile industry, as used as a biological stain in microbiology, histology and pathology applications, tracing agent, solar collector, paper and laser dye [47,48]. There is no report on the utilization of $NaBH_4$ assisted ZIF-8 synergistic degradation [49].

In this manuscript, a novel nanocrystalline mesoporous faujasite type metal-organic framework, ZIF-8 catalyst, has been synthesized through the green route and its $NaBH_4$ assisted room temperature rhodamine B degradation catalytic activity has been studied. Remediation of organic dyes from the effluents of textile industries in an economical fashion is a significant challenge for the textile industry. Hence the researchers developed many catalysts to remove the organic dyes from the effluents. The use of suitable catalysts for the reduced dyes is a promising technique among the recent developments. Here our ZIF-8 nanoparticles are used as a catalyst to degrade the RhB dye assisted by $NaBH_4$. The degradation products are confirmed through the LC-Mass spectroscopic technique. A Plausible catalytic reaction mechanism is also proposed.

2. Experimental

2.1. Materials and synthetic procedures

Zinc nitrate hexahydrate (≥98 %), CTAB (≥99 %), and 2-methylimidazole (99 %) were bought from Sigma-Aldrich are utilized as such without further purification.

2.2. Synthesis of bare ZIF-8 MOFs

In a typical synthesis, 1 mL of 2-methylimidazole (MeIm, 1.3 M) in water was stirred in a glass vial at 350 rpm at room temperature. Subsequently, 1 mL of $Zn(NO_3)_2{\cdot}6H_2O$ (0.025 M) in water was added, finally the addition of 1 mL of CTAB solution (0.16 mg/mL). The mixture was stirred for 2 min afterward, which was placed undisturbed at room temperature for three hours. After that, the solution turned turbid, indicating the formation of ZIF-8 [50]. The obtained nanoparticles were separated from the reaction mixture by using centrifugation at 6000 RCF

for 5 min. The ensuing particles were next washed with water two times and finally re-dispersed in water (3 mL).

solutions were made using double distilled water. The RhB dye degradation reaction was screened in a UV–vis spectrophotometer at 553 nm. This study was carried out in the presence and absence of the catalyst along with $NaBH_4$ at room temperature. The change in RhB concentra-

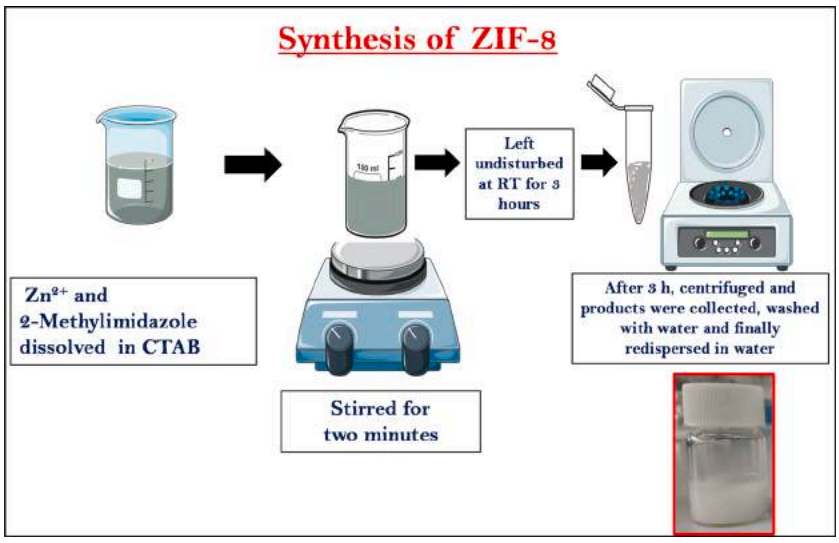

2.3. Characterization

The powder XRD patterns were recorded by utilizing Ultima IV diffractometer (M/s. Rigaku Corporation, Japan) with Ni- separated Cu Kα radiation source (λ = 1.54178 Å) at 30 mA and 40 kV and the resulting records were collected inside the 2θ range of 0.1−5° and 5−80° with a step size of 0.008° and a scan rate of 0.5° per minute. The morphological examinations were done by utilizing a field emission-scanning electron microscope (FE-SEM Zeiss Ultra Plus operated at 3 kV). 2 μl of this arrangement was then stored on a carbon film (400 mesh cooper) for the SEM. Transmission electron microscopy (TEM) pictures of the samples were investigated utilizing a JEOL JEM2100 TEM instrument (Australia) with speeding up the voltage of 200 kV. Dynamic light scattering (DLS) for calculation of particle size distribution was studied using a Zetasizer Nano ZSP-Malvern Panalytical instrument. Thermogravimetry /differential thermal examination (TG/DTA) contemplates were done utilizing STA 2500 Regulus NETZSCH, Japan instrument. The pore size and surface area of the samples were described under fluid nitrogen (77 K) temperature using (Quanta Chrome Nova-1000, USA) surface analyzer instrument. Additionally, pore volume and surface area of the nanoparticles were calculated by de Boer t-plot and Brunauer-Emmett-Teller (BET) strategies, separately. The samples were activated at 400 °C under a dynamic vacuum before the nitrogen adsorption/desorption analysis. Fourier transform infrared spectra (FT-IR) of samples were recorded on a PerkinElmer (Spectrum 100), USA instrument by using 1:10 KBr pellets with 10 number of scans at room temperature. UV–vis spectra of the samples were recorded by utilizing Perkin Elmer Lambda 25 UV–vis spectrophotometer. X-ray photoelectron spectroscopic (XPS) analysis data was obtained by using a Thermofisher scientific (theta probe spectrometer), UK instrument to find an elemental composition. The rhodamine B degraded products were analyzed by LC-ESI-MS (Waters 2695 Separation Module- ZORBAX Eclipse XDB-C18).

2.4. Catalytic degradation

Rhodamine B dye (RhB, Empirical Formula, $C_{28}H_{31}ClN_2O$, Molecular Weight, 479.01, ≥95 % purity purchased from Sigma-Aldrich, India) was used without any further purification, and the required diluted

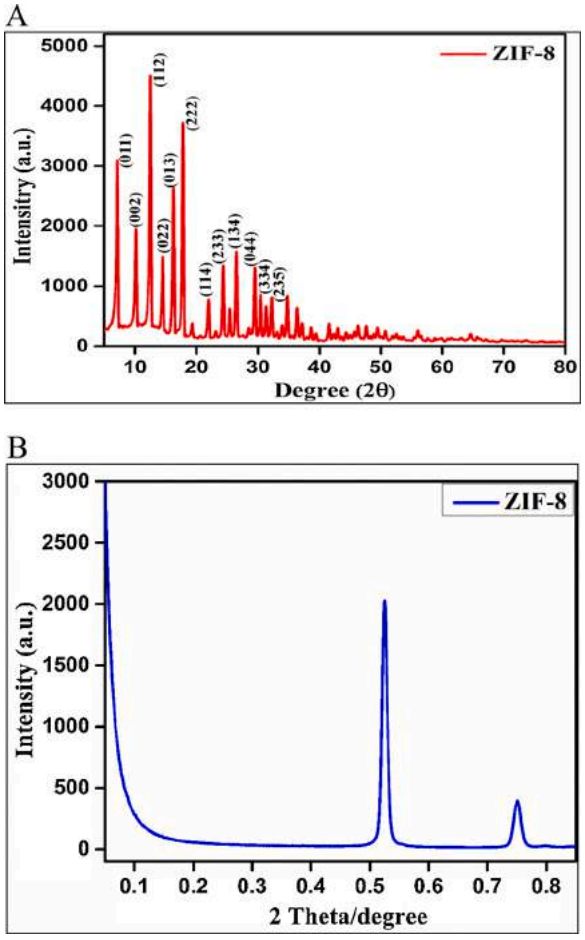

Fig. 1. A. Wide-angle X-ray diffraction patterns of ZIF-8. B. Low angle X-ray diffraction patterns of ZIF-8.

tion measures the resulting rate of the reaction. 10 μL of 1 mM aqueous solution of RhB was taken in a 3.5 ml quartz cuvette, and 810 μL of double-distilled water was added. After that, 80 μL of 0.1 M $NaBH_4$ solution and 100 μL aqueous suspension of ZIF-8 nanoparticles (6 mg/mL) was added to it. Upon reduction of RhB, the color of the mixture reduced gradually. The same process was repeated for the uncatalyzed reaction where instead of catalyst, 100 μL of double distilled water without catalyst was added to the reaction mixture to maintain the same above volume of the reaction mixture. The catalyzed and uncatalyzed reaction rate was measured by monitoring the change in the optical activity of RhB with time at 553 nm. All the kinetic studies reported in this work were carried out under normal conditions.

3. Results and discussion

3.1. X-ray diffraction pattern

The well-resolved highly crystalline XRD patterns of the samples are shown in Fig. 1 and Fig. S1 to confirm the successful synthesis of ZIF-8 using the sol-gel method. The XRD patterns of the sample contain the characteristic sharp peaks at $2\theta = 0.53^\circ$, 0.75°, 7.16°, 10.18°,12.52°, 14.5°, 16.24°, 17.84°, and 19.28°. The XRD pattern of the as-synthesized sample was compared with the ones reported in the literature (JCPDS 00-062-1030) to confirm a cubic lattice (space group I43 m) and a mesoporous faujasite zeolite topology of the synthesized product [51, 52].

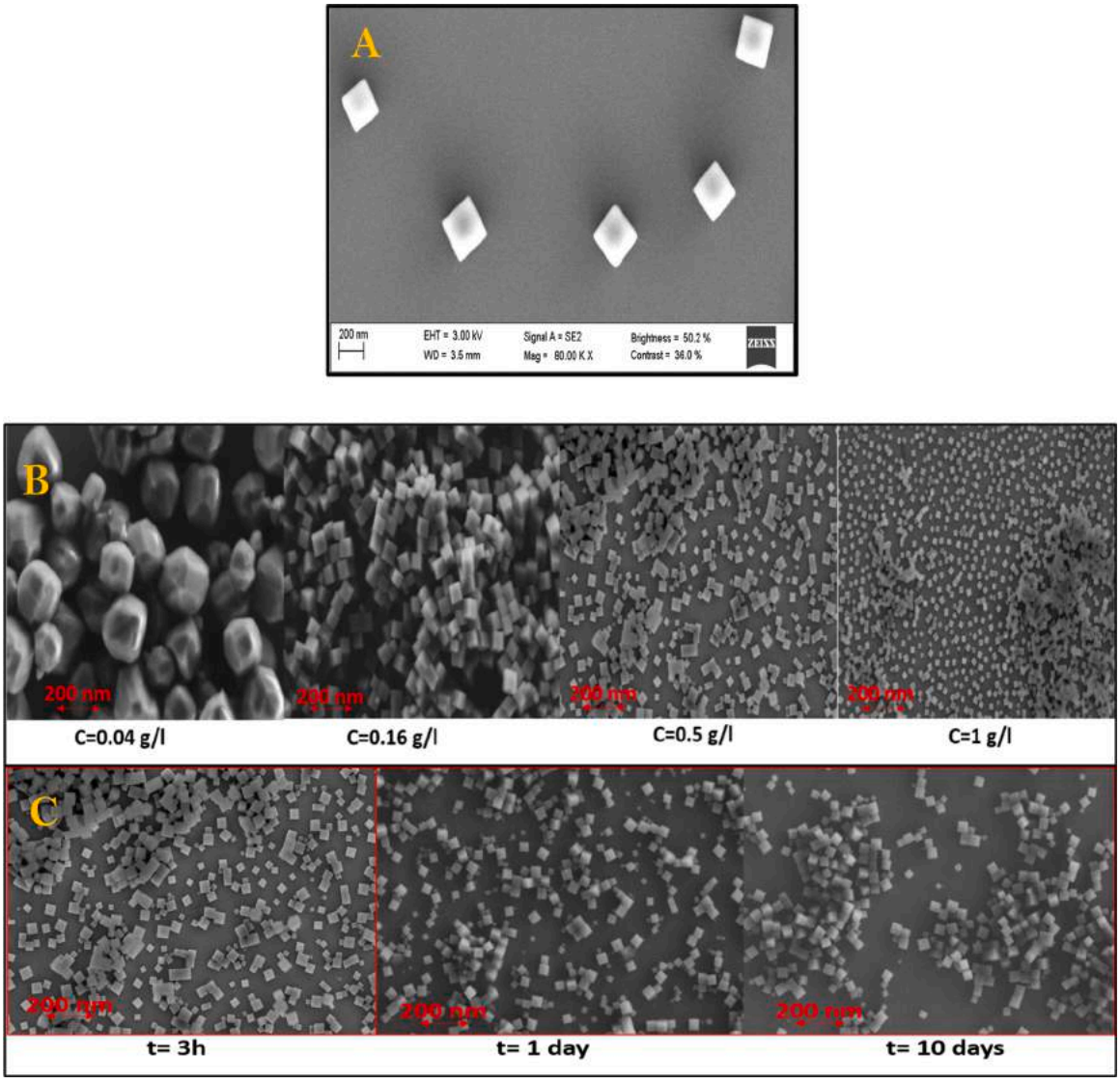

Fig. 2. (A) FE-SEM analysis of ZIF-8 (B) SEM analysis of ZIF-8 with various concentrations of CTAB, and (C) SEM analysis of ZIF-8 stability with multiple time intervals.

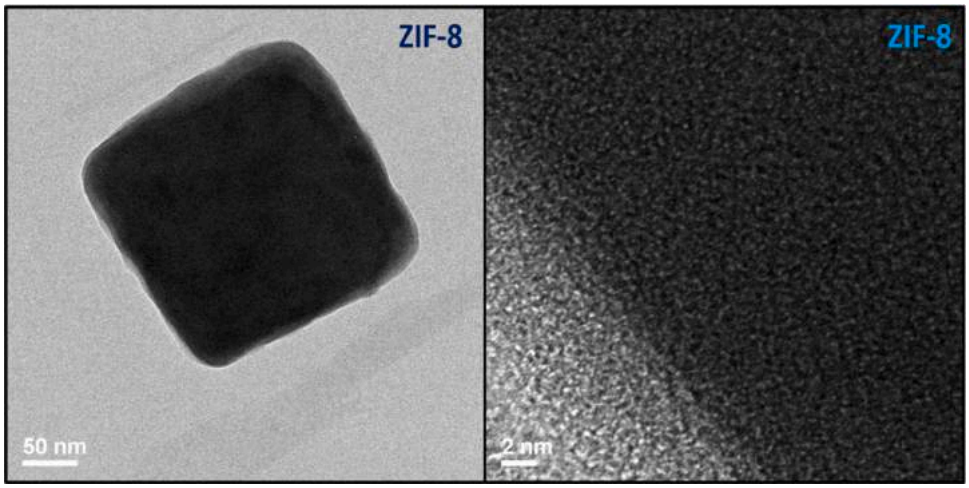

Fig. 3. The TEM analysis of ZIF-8.

Table 1
Results of the DLS of various samples obtained by varying the concentration of the CTAB in the dissolution.

C (CTAB) (mg/mL)	NP size (nm)	PDI (nm)
0.01	1305	0.37
0.02	762	0.61
0.04	655	0.17
0.08	332	0.055
0.16	130	0.11
0.25	127	0.081
0.50	116	0.033
0.75	82	0.018
1.00	66	0.017
1.50	52	0.075
1.80	51	0.099

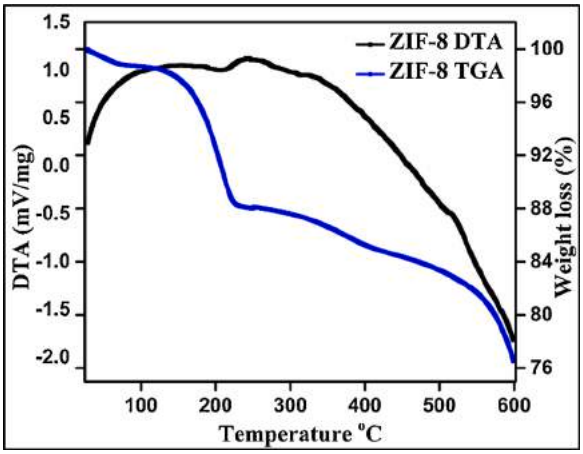

Fig. 4. Thermogravimetric/differential thermal analysis of ZIF-8.

3.2. Scanning electron microscopic analysis

Scanning electron microscopic (FE-SEM) analysis was carried out by preparing dissolutions ranging from 1:2 to 1:10 depending on the initial surfactant concentration of the sample. The size and shape of the nano MOF were characterized and compared with the values obtained from the DLS experiments. Fig. 2 shows the representative FE-SEM images of ZIF-8, which were homogeneously distributed, and exhibited rhombic dodecahedron shape, due to the cationic surfactant. In our synthesis

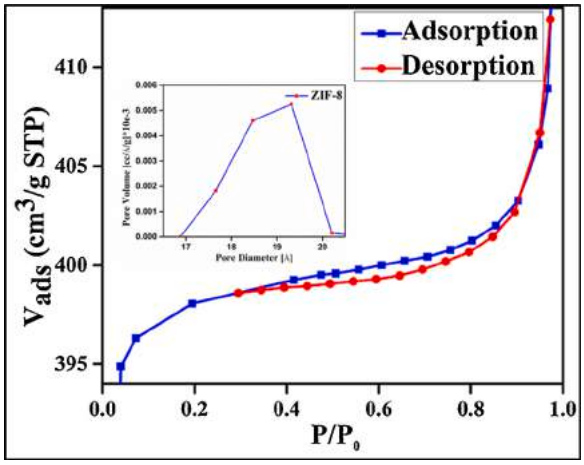

Fig. 5. N_2 adsorption/desorption curve and pore size distribution of ZIF-8.

procedure, we used Cetyl hexadecyltrimethylammonium bromide (CTAB) as the template, which is very useful in regulating the size and shape of ZIF-8 nanoparticles, particularly in the aqueous medium. This is possibly due to the vast hydrophobic saturated alkyl chain of CTAB, and that can be adsorbed by the similar hydrophobic surface of the ZIF-8 crystals in the aqueous solution. Also, CTAB functions as a capping agent and slows down the crystallization process, which leads to the formation of ZIF-8 particles with cubic morphology. From these results, it is found that CTAB is the most effective control for the synthesis of the catalyst [53,54]. It is observed from the above characterization that as the concentration of the CTAB increases, the size of the particles decreases. The particles were found to be stable for more than ten days, and no change in the size and shape of the particles was observed.

3.3. TEM analysis

Fig. 3 shows the particle size and shape of the synthesized mesoporous faujasite type ZIF-8 catalyst. Around 500 nm size, cuboids are observed from the analysis. However, the particle size is not uniform. The HRTEM analysis shows the cross-linked hexagonal framework of the synthesized mesoporous materials.

3.4. Dynamic light scattering

DLS is used to characterize the hydrodynamic size and the

Table 2
Textural properties of ZIF-8.

Material	S_{BET} (m^2 g^{-1})	Pore size (Å)	Pore volume (cm^3 g^{-1})
ZIF-8	1622	21.319	0.460

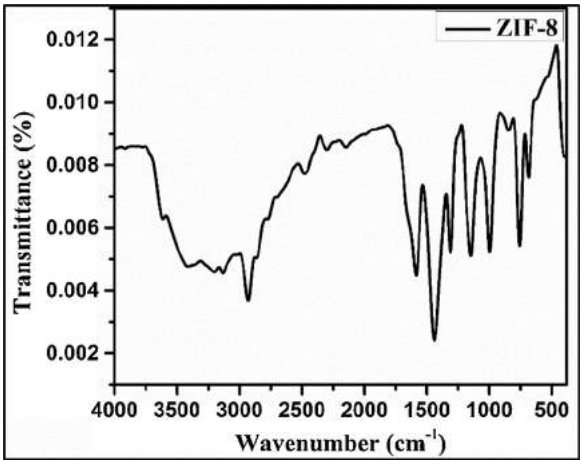

Fig. 6. FT-IR analysis of ZIF-8.

polydispersity index (PDI) of ZIF-8 nanoparticles. It was found that CTAB plays a crucial role in regulating the size of the particle. As the concentration of CTAB increases, the size of the particles decreases, as shown in the Table 1.

The size and PDI of the ZIF-8 decreases as the concentration of CTAB in the synthesis increases. It may be due to the reason that CTAB caps up the particles. Since it is hydrophobic, it repels the water molecules and this reduces the size of the resulting MOF particles.

3.5. Thermogravimetry/differential thermal analysis

To contemplate the thermal stability of the ZIF-8 sample, TG/DTA was performed under a nitrogen environment to know the thermal stability of the synthesized ZIF-8, and the resulting result was placed as Fig. 4. From the analysis, there are weight losses at three different temperature regions, which are at <100 °C, 100−300 °C, the third weight reduction beginning from 550 °C. The initial weight loss <100 °C may be attributed to the loss of adsorbed water molecules and the solvent molecules present in the sample, the other weight reduction at 100−300 °C is because of the oxidative decomposition of 2-MeImz and the weight reduction beginning from 550 °C could be ascribed to the degradation of the organic linkers in ZIF-8 crystal. From the DTA curve we can observe three peaks the first one is endothermic and the rest of the two are exothermic. The first endothermic peak at 200 deg is due to the dissolution of the solvent molecules, the second peak around 280 deg this is due to the oxidative the disintegration of 2-MeImz and the last exothermic peak appeared at 530 deg this is due to the dissolution of the organic linkers and ZIF-8 crystal [55,56].

3.6. BET-surface area

To calculate the surface area and the pore size distribution, N_2 adsorption/desorption isotherms for these ZIF-8 MOFs were recorded (Fig. 5). The Brunauer-Emmett-Teller (BET) surface areas and total pore

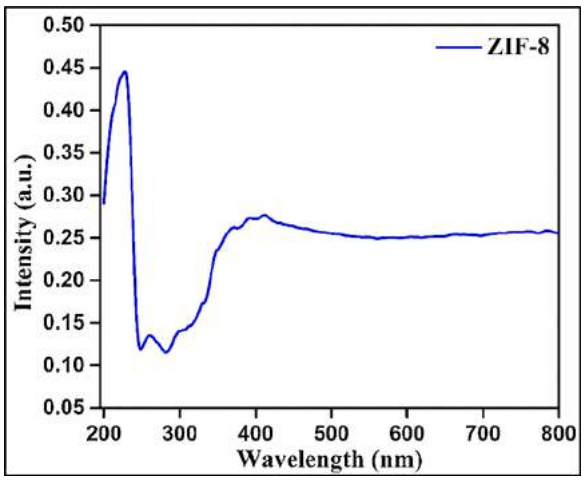

Fig. 7. UV–vis-DRS analysis of ZIF-8.

volumes are found to be 1622 m^2 g^{-1} and 0.46 cm^3 g^{-1}, respectively. The textural properties of the sample are mentioned in Table 2 and Fig. 5 shows pore size distribution and N_2 adsorption/desorption isotherm of the composite sample. The sample exhibits a typical type IV N_2 adsorption isotherm with an H_4 kind hysteresis loop in the range of P/P_0 = 0.4–0.8, demonstrating a mesoporous structure [57].

3.7. Fourier transform infrared spectroscopic analysis

FT-IR study shows the similarities of the ZIF-8 (Fig. 6) framework with Faujasite [58]. The characteristic bands in the region of 500−1500 cm^{-1}; 1438 cm^{-1} and 1296 cm^{-1} are due to CN— stretching, and at 1115 cm^{-1} and between the 900−700 cm^{-1} are due to bending vibrations of C—H bond. The bands at 2915 cm^{-1} and 2857 cm^{-1} are caused by the C–H stretching vibration of methyl and methylene groups of CTAB. In the ZIF-8, the only band that seems to remain in the 2915 cm^{-1} one; the presence of remaining CTAB cannot be varied, but this is unlikely as the concentration of CTAB during the synthesis was low under the critical micellar concentration and before it, it was cleaned several times with MQ water.

The peaks at 898 and 987 cm^{-1} represent the CO— stretching vibration on the Zn—OC— bond. The peaks at 3400 and 2929 cm^{-1} represent stretching vibrations of the C—H bond in the imidazole ring. The major peak at 1584 cm^{-1} is a result of the stretching vibration of the C═N group. The peaks at 600-1500 cm^{-1} represent the entire ring stretching or bending, and the major peak at 422 cm^{-1} is attributed to the stretching vibration of the Zn–N group of the ZIF-8 framework [59].

3.8. UV–vis-DRS analysis

Fig. 7 shows the Ultraviolet-Visible diffuse reflectance spectroscopic analysis of a novel mesoporous faujasite type ZIF-8 catalyst. It shows a major peak around 240 nm and a minor peak at around 260 nm are due to the free ionic species and a broad peak around 380 nm is due to the tetrahedrally coordinated Zn^{4+} species with redshift.

3.9. X-ray photoelectron spectroscopy analysis

The structure of ZIF-8 was also confirmed by XPS analysis. Fig. 6 displays the survey spectrum of ZIF-8. In the C1s, N1s, and O1s region (Fig. 8 and Fig. S2), three signals around 285 eV for C1s, 398.93 eV for

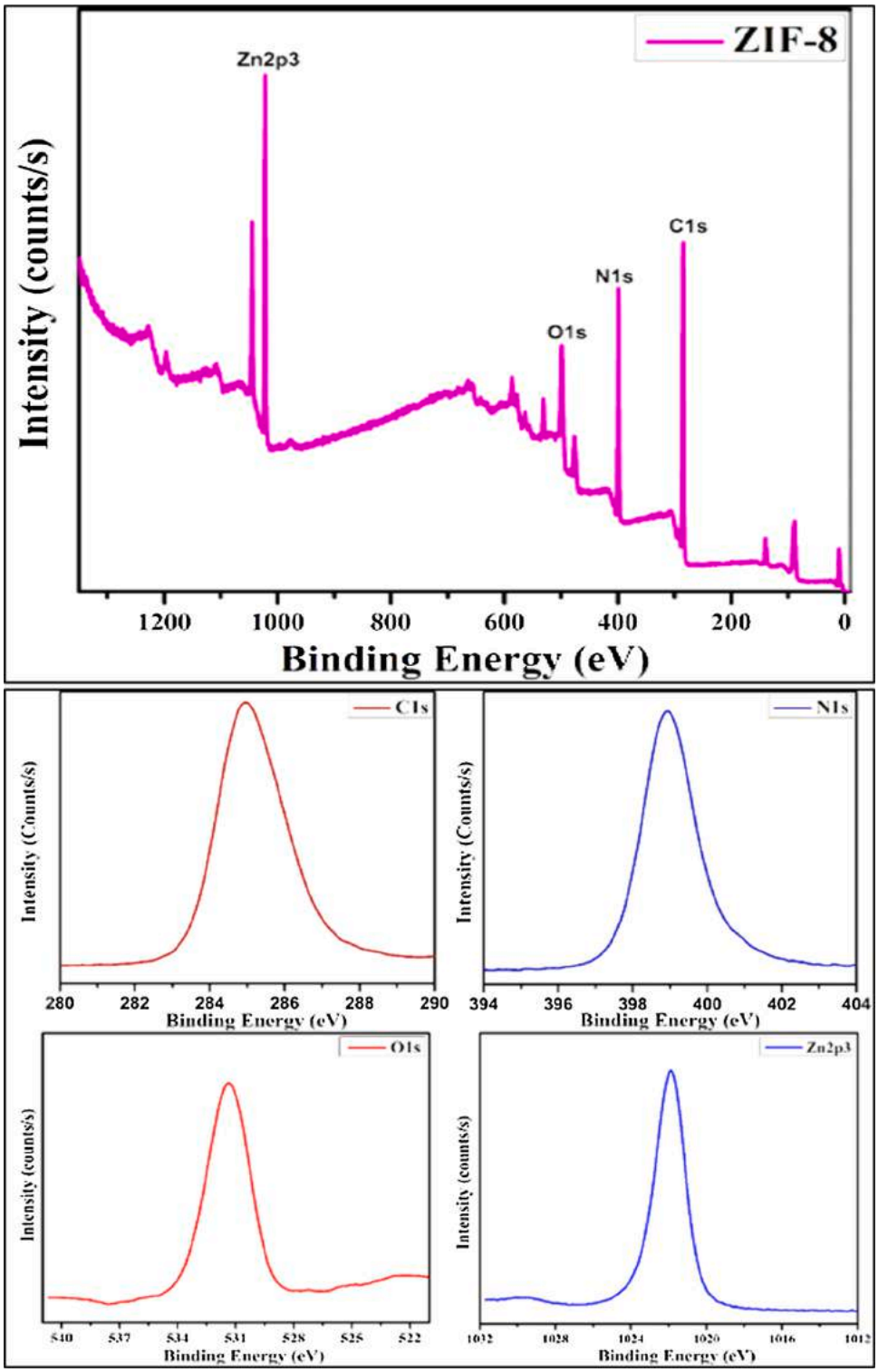

Fig. 8. XPS analysis of ZIF-8.

Table 3
Quantitative Results of XPS Analysis for ZIF-8.

Sample	Name	Peak BE	FWHM eV	Area (P) CPS.eV	Atomic %	No. of atoms
ZIF-8	C 1s	285.00	2.03	144042.97	62.3	11.8154
	N 1s	398.93	1.60	95393.65	26.5	4.3
	O 1s	531.32	2.36	15715.41	2.8	0.398
	Zn $2p^3$	1021.89	1.84	206545.03	8.4	0.292

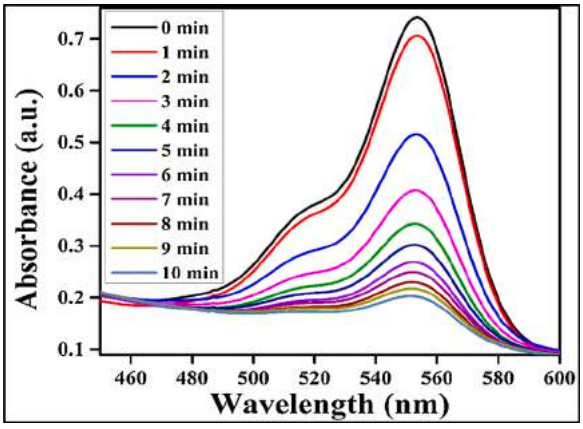

Fig. 9. UV–vis spectroscopic analysis of the degradation of RhB by $NaBH_4$ assisted ZIF-8 nanoparticles at 553 nm (max of RhB).

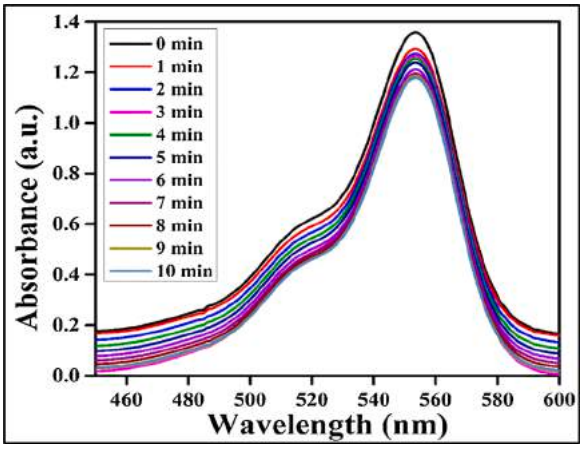

Fig. 10. UV–vis spectroscopic analysis of the RhB degradation by $NaBH_4$ in the absence of the ZIF-8 catalyst at 553 nm.

N1s, and 531.32 eV for O1s are observed respectively, which are belongs to C and N present in the ligand. [60–64]. In the zinc region, the peak observed at 1021.89 eV ($Zn2p^3$), revealed that the presence of Zn^{4+}. All binding energy values and related areas are mentioned in Table 3.

3.10. ZIF-8 nanoparticles catalytic, $NaBH_4$ assisted rhodamine B degradation

In general, dye degradation is taking place around one hour. However, when we used the synthesized ZIF-8 nanoparticles along with $NaBH_4$ as the reducing agent, it was reduced within ten minutes, which

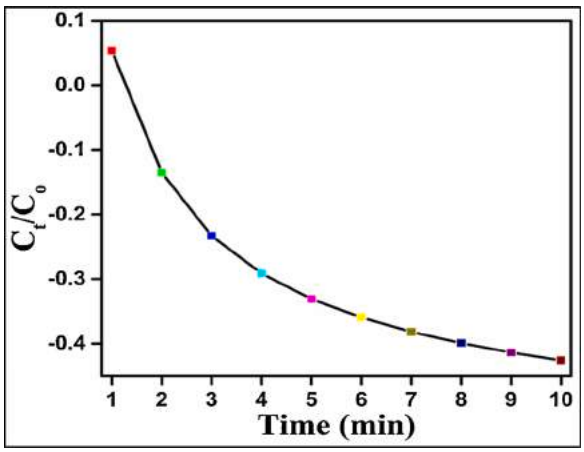

Fig. 11. UV–vis kinetic analysis of the RhB degradation by $NaBH_4$ assisted ZIF-8 nanoparticles.

is a significant advantage [65–67]. The RhB dye degradation reaction was screened in a UV–vis spectrophotometer at 553 nm. This study was carried out in the presence and absence of the catalyst and $NaBH_4$ at room temperature. The change in RhB concentration measures the resulting reaction rate of the reaction, and the results are given in Figs. 9–11. The catalytic activity is retained even for two different cycles of the catalyst.

3.10.1. Kinetic studies of rhodamine B (RhB) degradation in presence of ZIF-8 and $NaBH_4$

C_o is the Initial concentration of Rhodamine B. C_t is the concentration of Rhodamine B after time t. The concentration of the dye decreases with time t. This follows the first-order rate of decomposition. It reaches the maximum decomposition at 10 min. This is a significant development in the catalytic field (Fig. 12).

The catalytic degradation mechanism of organic dye, rhodamine B by ZIF-8 catalyst was studied by using Liquid chromatography-mass spectrometry (LC–MS), and the components of degradation products were analyzed. The outcomes after rhodamine B degradation were recognized by positive ion mode mass spectra after 10 min of reaction in the presence and absence of the ZIF-8 catalyst. The mass peak at *m/z* 443 was observed for the initial analyte solution and is attributed to the rhodamine B molecule of a Cl^- ion. The peak at *m/z* 414 was assigned to the de ethylated intermediates and chromophore cleavages of rhodamine B. The ZIF-8 free reaction did not give any fragmentation. The fragmentation is possible due to the H^+ ions adsorbed over the Zn^{2+} atoms (Fig. 13).

4. Conclusion

In the present study, a new nano-crystalline mesoporous faujasite type ZIF-8 nanoparticles are synthesized in the solution phase at normal room temperature. The ZIF-8 was characterized by PXRD, SEM, TEM, DLS, TG-DTA, BET, FT-IR, UV–vis, and XPS techniques. RhB dye was degraded by ~ 95 % in 10 min over the $NaBH_4$ assisted ZIF-8. The degradation follows first-order kinetics. The prepared ZIF-8 is a reusable catalyst over two cycles. It is noteworthy that this method is simple, easy to handle, safe, and cost-effective. Thus, it has the potential to be a beneficial technology for environmental remediation.

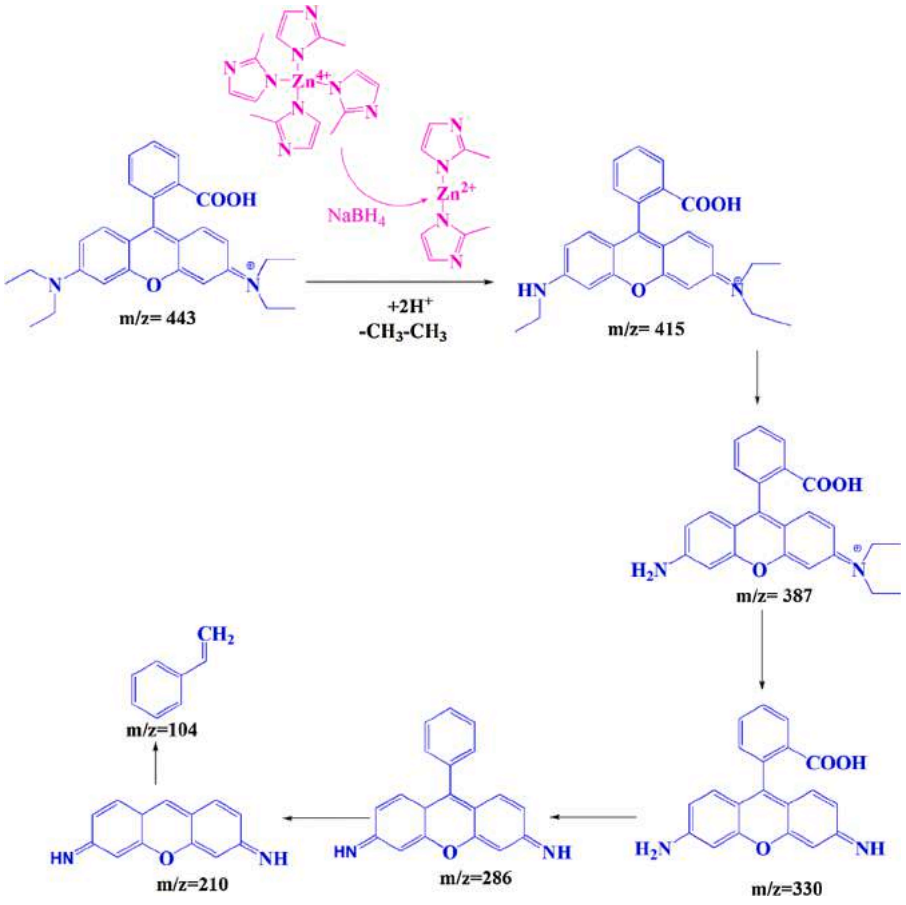

Fig. 12. Mechanism of Rhodamine B dye degradation.

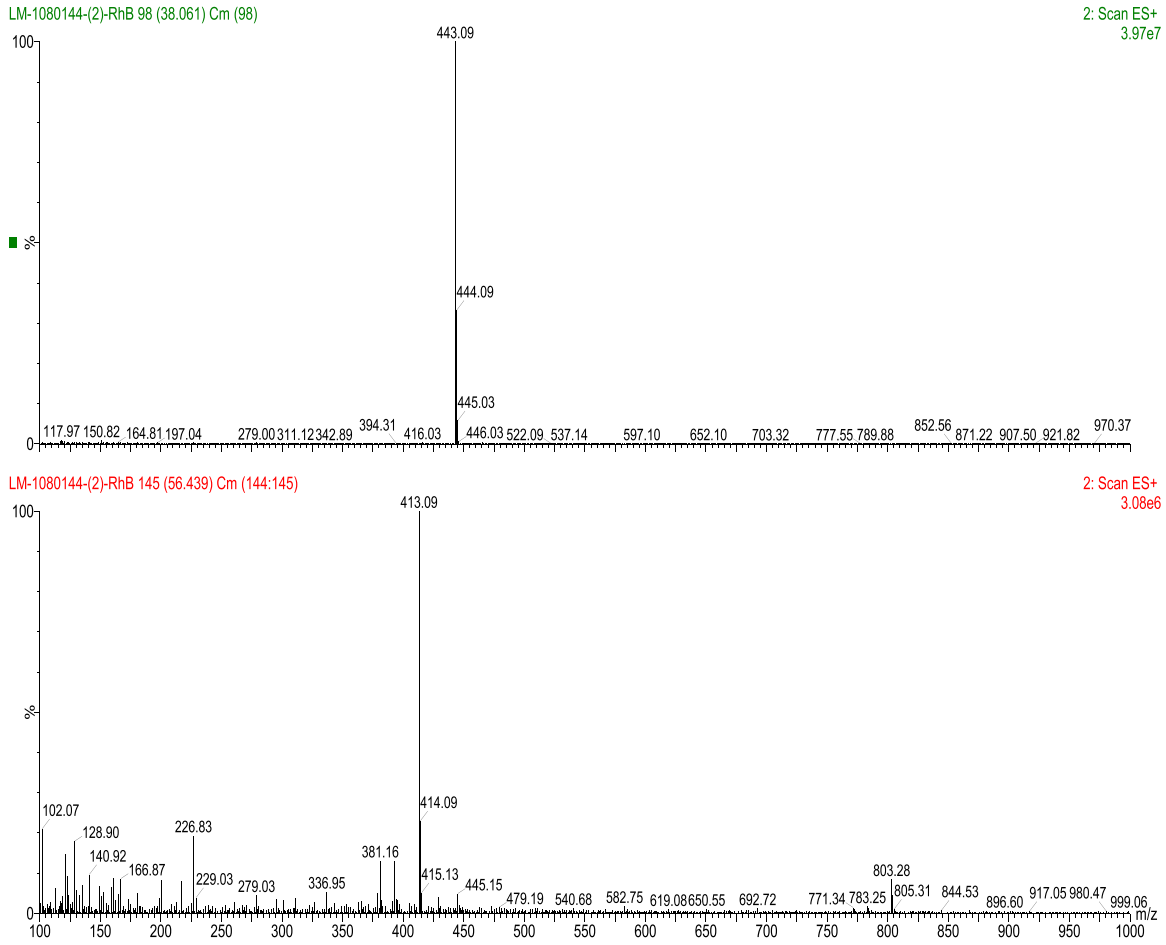

Fig. 13. The LC–MS analysis of rhodamine B dye degradation in the presence and absence of the ZIF-8 catalyst.

Declaration of Competing Interest

The authors declare that they have no known competing financial interests or personal relationships that could have appeared to influence the work reported in this paper.

Acknowledgments

We thank the Department of Science and Technology-Science and Engineering Research Board, New Delhi, Govt. of India, (Grant number EMR/2014/000629), for the financial support of and one of the authors, Suman Chirra, gratefully thank the Ministry of Human Resource and Development (MHRD), New Delhi for financial support.

Appendix A. Supplementary data

Supplementary material related to this article can be found, in the online version, at doi:https://doi.org/10.1016/j.mtcomm.2020.101993.

References

[1] J.L.C. Rowsell, O.M. Yaghi, Strategies for hydrogen storage in metal-organic frameworks, Angew. Chem. Int. Ed. 44 (30) (2005) 4670–4679.
[2] D. Britt, H. Furukawa, B. Wang, T.G. Glover, O.M. Yaghi, Highly efficient separation of carbon dioxide by a metal-organic framework replete with open metal sites, Proc. Natl. Acad. Sci. 106 (49) (2009) 20637–20640.
[3] J.-R. Li, R.J. Kuppler, H.-C. Zhou, Selective gas adsorption and separation in metal-organic frameworks, Chem. Soc. Rev. 38 (5) (2009) 1477.
[4] L.J. Murray, M. Dincă, J.R. Long, Hydrogen storage in metal-organic frameworks, Chem. Soc. Rev. 38 (5) (2009) 1294.
[5] A.R. Millward, O.M. Yaghi, Metal−organic frameworks with exceptionally high capacity for storage of carbon dioxide at room temperature, J. Am. Chem. Soc. 127 (51) (2005) 17998–17999.
[6] A.C. McKinlay, R.E. Morris, P. Horcajada, G. Férey, R. Gref, P. Couvreur, C. Serre, BioMOFs: metal-organic frameworks for biological and medical applications, Angew. Chem. Int. Ed. 49 (36) (2010) 6260–6266.
[7] M.D. Allendorf, C.A. Bauer, R.K. Bhakta, R.J.T. Houk, Luminescent metal-organic frameworks, Chem. Soc. Rev. 38 (5) (2009) 1330.
[8] L.B. Vilhelmsen, K.S. Walton, D.S. Sholl, Structure and mobility of metal clusters in MOFs: Au, Pd, and AuPd clusters in MOF-74, J. Am. Chem. Soc. 134 (30) (2012) 12807–12816.
[9] D. Farrusseng, S. Aguado, C. Pinel, Metal-organic frameworks: opportunities for catalysis, Angew. Chem. Int. Ed. 48 (41) (2009) 7502–7513.
[10] J. Lee, O.K. Farha, J. Roberts, K.A. Scheidt, S.T. Nguyen, J.T. Hupp, Metal-organic framework materials as catalysts, Chem. Soc. Rev. 38 (5) (2009) 1450.
[11] P. Horcajada, C. Serre, M. Vallet-Regí, M. Sebban, F. Taulelle, G. Férey, Metal-organic frameworks as efficient materials for drug delivery, Angew. Chem. Int. Ed. 45 (36) (2006) 5974–5978.
[12] K.M.L. Taylor-Pashow, J. Della Rocca, Z. Xie, S. Tran, W. Lin, Postsynthetic modifications of iron-carboxylate nanoscale metal−organic frameworks for imaging and drug delivery, J. Am. Chem. Soc. 131 (40) (2009) 14261–14263.
[13] P. Horcajada, T. Chalati, C. Serre, B. Gillet, C. Sebrie, T. Baati, R. Gref, Porous metal–organic-framework nanoscale carriers as a potential platform for drug delivery and imaging, Nat. Mater. 9 (2) (2009) 172–178.
[14] B. Wang, A.P. Côté, H. Furukawa, M. O'Keeffe, O.M. Yaghi, Colossal cages in zeolitic imidazolate frameworks as selective carbon dioxide reservoirs, Nature 453 (7192) (2008) 207–211.
[15] S. Keskin, T.M. van Heest, D.S. Sholl, Can metal-organic framework materials play a useful role in large-scale carbon dioxide separations? ChemSusChem 3 (8) (2010) 879–891.
[16] G. Zhang, S. Hou, H. Zhang, W. Zeng, F. Yan, C.C. Li, H. Duan, High-performance and ultra-stable lithium-ion batteries based on MOF-derived ZnO@ZnO quantum Dots/C core-shell nanorod arrays on a carbon cloth anode, Adv. Mater. 27 (14) (2015) 2400–2405.
[17] A. Phan, C.J. Doonan, F.J. Uribe-Romo, C.B. Knobler, M. O'Keeffe, O.M. Yaghi, Synthesis, structure, and carbon dioxide capture properties of zeolitic imidazolate frameworks, Acc. Chem. Res. 43 (1) (2010) 58–67.

[18] R. Banerjee, A. Phan, B. Wang, C. Knobler, H. Furukawa, M. O'Keeffe, O.M. Yaghi, High-throughput synthesis of zeolitic imidazolate frameworks and application to CO2 capture, Science 319 (5865) (2008) 939–943.
[19] K.S. Park, Z. Ni, A.P. Cote, J.Y. Choi, R. Huang, F.J. Uribe-Romo, O.M. Yaghi, Exceptional chemical and thermal stability of zeolitic imidazolate frameworks, Proc. Natl. Acad. Sci. 103 (27) (2006) 10186–10191.
[20] M. Thomas, B.N. Nair, G.M. Anilkumar, A.P. Mohamed, K.G.K. Warrier, U. S. Hareesh, Processing of thermally stable 3D hierarchical ZIF-8@ZnO structures and their CO2 adsorption studies, J. Environ. Chem. Eng. 4 (2) (2016) 1442–1450.
[21] M. Jiang, X. Cao, D. Zhu, Y. Duan, J. Zhang, Hierarchically porous N-doped carbon derived from ZIF-8 nanocomposites for electrochemical applications, Electrochim. Acta 196 (2016) 699–707.
[22] J. Li, N. Wang, H. Yan, S. Ji, G. Zhang, Designing superhydrophobic surfaces with SAM modification on hierarchical ZIF-8/polymer hybrid membranes for efficient bio alcohol pervaporation, RSC Adv. 4 (104) (2014) 59750–59753.
[23] R. Banerjee, H. Furukawa, D. Britt, C. Knobler, M. O'Keeffe, O.M. Yaghi, Control of pore size and functionality in isoreticular zeolitic imidazolate frameworks and their carbon dioxide selective capture properties, J. Am. Chem. Soc. 131 (11) (2009) 3875–3877.
[24] Y.-S. Li, F.-Y. Liang, H. Bux, A. Feldhoff, W.-S. Yang, J. Caro, Molecular sieve membrane: supported metal-organic framework with high hydrogen selectivity, Angew. Chem. Int. Ed. 49 (3) (2009) 548–551.
[25] C. Chizallet, S. Lazare, D. Bazer-Bachi, F. Bonnier, V. Lecocq, E. Soyer, A.-A. Quoineaud, N. Bats, Catalysis of transesterification by a nonfunctionalized metal−organic framework: acido-basicity at the external surface of ZIF-8 probed by FTIR and initiocalculations, J. Am. Chem. Soc. 132 (35) (2010) 12365–12377.
[26] G. Lu, J.T. Hupp, Metal−organic frameworks as sensors: a ZIF-8 based Fabry−Pérot device as a selective sensor for chemical vapors and gases, J. Am. Chem. Soc. 132 (23) (2010) 7832–7833.
[27] C. Davey, D. Leak, D. Patterson, Hybrid and mixed matrix membranes for separations from fermentations, Membranes 6 (1) (2016) 17.
[28] J. Gascon, S. Aguado, F. Kapteijn, Manufacture of dense coatings of Cu3(BTC)2 (HKUST-1) on α-alumina, Microporous Mesoporous Mater. 113 (1–3) (2008) 132–138.
[29] Y. Pan, Y. Liu, G. Zeng, L. Zhao, Z. Lai, Rapid synthesis of zeolitic imidazolate framework-8 (ZIF-8) nanocrystals in an aqueous system, Chem. Commun. 47 (7) (2011) 2071.
[30] R. Ameloot, E. Gobechiya, H. Uji-i, J.A. Martens, J. Hofkens, L. Alaerts, B.F. Sels, D. E. De Vos, Direct patterning of oriented metal-organic framework crystals via control over crystallization kinetics in clear precursor solutions, Adv. Mater. 22 (24) (2010) 2685–2688.
[31] X.-C. Huang, Y.-Y. Lin, J.-P. Zhang, X.-M. Chen, Ligand-directed strategy for zeolite-type metal-organic frameworks: zinc(II) imidazolates with unusual zeolitic topologies, Angew. Chem. Int. Ed. 45 (10) (2006) 1557–1559.
[32] S.K. Nune, P.K. Thallapally, A. Dohnalkova, C. Wang, J. Liu, G.J. Exarhos, Synthesis and properties of nano zeolitic imidazolate frameworks, Chem. Commun. 46 (27) (2010) 4878.
[33] N.P. Raval, P.U. Shah, N.K. Shah, Adsorptive amputation of hazardous azo dye Congo red from wastewater: a critical review, Environ. Sci. Pollut. Res. - Int. 23 (15) (2016) 14810–14853.
[34] M.A.M. Salleh, D.K. Mahmoud, W.A. Karim, A. Idris, Cationic and anionic dye adsorption by agricultural solid wastes: a comprehensive review, Desalination 280 (1–3) (2011) 1–13.
[35] S. Khamparia, D. Jaspal, Investigation of adsorption of Rhodamine B onto a natural adsorbent Argemone mexicana, J. Environ. Manage. 183 (2016) 786–793.
[36] B. Royer, N.F. Cardoso, E.C. Lima, T.R. Macedo, C. Airoldi, A useful organofunctionalized layered silicate for textile dye removal, J. Hazard. Mater. 181 (1–3) (2010) 366–374.
[37] M. Oveisi, M. Alinia Asli, N.M. Mahmoodi, Carbon nanotube-based metal-organic framework nanocomposites: synthesis and their photocatalytic activity for decolorization of colored wastewater, Inorg. Chim. Acta 487 (2019) 169–176.
[38] N.M. Mahmoodi, J. Abdi, M. Taghizadeh, A. Taghizadeh, B. Hayati, A.A. Shekarchi, M. Vossoughi, Activated carbon/metal-organic framework nanocomposite: preparation and photocatalytic dye degradation mathematical modeling from wastewater by least squares support vector machine, J. Environ. Manage. 233 (2019) 660–672.
[39] N.M. Mahmoodi, M. Taghizadeh, A. Taghizadeh, Ultrasound-assisted green synthesis and application of the recyclable nanoporous chromium-based metal-organic framework, Korean J. Chem. Eng. 36 (2) (2018) 287–298.
[40] G. Li Puma, F. Machuca-Martínez, M. Mueses, J. Colina-Márquez, C. Bustillo-Lecompte, In Advanced Oxidation Processes - Applications, Trends, and Prospects, IntechOpen, 2020.
[41] N.M. Mahmoodi, M. Oveisi, A. Taghizadeh, M. Taghizadeh, Novel magnetic amine-functionalized carbon nanotube/metal-organic framework nanocomposites: from green ultrasound-assisted synthesis to detailed selective pollutant removal modeling from binary systems, J. Hazard. Mater. 368 (2019) 746–759.
[42] A.K. Verma, R.R. Dash, P. Bhunia, A review of chemical coagulation/flocculation technologies for removal of color from textile wastewaters, J. Environ. Manage. 93 (1) (2012) 154–168.
[43] K.-Y.A. Lin, C.-H. Wu, Efficient adsorptive removal of toxic amaranth dye from water using a zeolitic imidazolate framework, Water Environ. Res. 90 (11) (2018) 1947–1955.
[44] H. Li, M. Eddaoudi, M. O'Keeffe, O.M. Yaghi, Design and synthesis of an exceptionally stable and highly porous metal-organic framework, Nature 402 (6759) (1999) 276–279.
[45] J.L.C. Rowsell, O.M. Yaghi, Metal-organic frameworks: a new class of porous materials, Microporous Mesoporous Mater. 73 (1–2) (2004) 3–14.
[46] C. Stabler, E. Ionescu, M. Graczyk-Zajac, I. Gonzalo-Juan, R. Riedel, Silicon oxycarbide glasses and glass-ceramics: "all-rounder" materials for advanced structural and functional applications, J. Am. Ceram. Soc. 101 (11) (2018) 4817–4856.
[47] J. Zhang, X. Hu, X. Yan, R. Feng, M. Zhou, J. Xue, Enhanced adsorption of Rhodamine B by magnetic nitrogen-doped porous carbon prepared from bimetallic ZIFs, Colloids Surf. A Physicochem. Eng. Asp. 575 (2019) 10–17.
[48] Y. Li, K. Zhou, M. He, J. Yao, Synthesis of ZIF-8 and ZIF-67 using mixed-base and their dye adsorption, Microporous Mesoporous Mater. 234 (2016) 287–292.
[49] B. Chen, Z. Yang, Y. Zhu, Y. Xia, Zeolitic imidazolate framework materials: recent progress in synthesis and applications, J. Mater. Chem. A 2 (40) (2014) 16811–16831.
[50] Y. Wu, M. Zhou, B. Zhang, B. Wu, J. Li, J. Qiao, F. Li, Amino acid assisted templating synthesis of hierarchical zeolitic imidazolate framework-8 for efficient arsenate removal, Nanoscale 6 (2) (2014) 1105–1112.
[51] X. Hu, X. Yan, M. Zhou, S. Komarneni, One-step synthesis of nanostructured mesoporous ZIF-8/silica composites, Microporous Mesoporous Mater. 219 (2016) 311–316.
[52] Z. Zhang, S. Xian, Q. Xia, H. Wang, Z. Li, J. Li, Enhancement of CO2 adsorption and CO2/N2 selectivity on ZIF-8 via postsynthetic modification, Aiche J. 59 (6) (2013) 2195–2206.
[53] Y. Pan, D. Heryadi, F. Zhou, L. Zhao, G. Lestari, H. Su, Z. Lai, Tuning the crystal morphology and size of zeolitic imidazolate framework-8 in aqueous solution by surfactants, CrystEngComm 13 (23) (2011) 6937.
[54] G. Zheng, Z. Chen, K. Sentosun, I. Pérez-Juste, S. Bals, L.M. Liz-Marzán, M. Hong, Shape control in ZIF-8 nanocrystals and metal nanoparticles@ZIF-8 heterostructures, Nanoscale 9 (43) (2017) 16645–16651.
[55] L. Zhang, G. Qian, Z. Liu, Q. Cui, H. Wang, H. Yao, Adsorption and separation properties of n-pentane/isopentane on ZIF-8, Sep. Purif. Technol. 156 (2015) 472–479.
[56] K. Kida, M. Okita, K. Fujita, S. Tanaka, Y. Miyake, Formation of high crystalline ZIF-8 in an aqueous solution, CrystEngComm 15 (9) (2013) 1794.
[57] J. Cravillon, S. Münzer, S.-J. Lohmeier, A. Feldhoff, K. Huber, M. Wiebcke, Rapid room-temperature synthesis and characterization of nanocrystals of a prototypical zeolitic imidazolate framework, Chem. Mater. 21 (8) (2009) 1410–1412.
[58] Rosemarie Szostak, Handbook of Molecular Sieves, Van Nostrand Reinhold, New York, 1992.
[59] Y. Pan, D. Heryadi, F. Zhou, L. Zhao, G. Lestari, H. Su, Z. Lai, Tuning the crystal morphology and size of zeolitic imidazolate framework-8 in aqueous solution by surfactants, CrystEngComm 13 (23) (2011) 6937.
[60] S. Chirra, S. Siliveri, R. Gangalla, S. Goskula, S.R. Gujjula, A.K. Adepu, V. Narayanan, Synthesis of new multivalent metal ion functionalized mesoporous silica and studies of their enhanced antimicrobial and cytotoxicity activities, J. Mater. Chem. B 7 (45) (2019) 7235–7245.
[61] S. Chirra, S. Siliveri, A.K. Adepu, S. Goskula, S.R. Gujjula, V. Narayanan, Pd-KIT-6: synthesis of a novel three-dimensional mesoporous catalyst and studies on its enhanced catalytic applications, J. Porous Mater. 26 (6) (2019) 1667–1677.
[62] A.K. Adepu, S. Siliveri, S. Chirra, S. Goskula, S.R. Gujjula, R. Anumula, V. Narayanan, A novel porous Fe3O4/Titanosilicate/g-C3N4 ternary nanocomposites: synthesis, characterization, and their enhanced photocatalytic activity on Rhodamine B degradation under sunlight irradiation, J. Water Process. Eng. 34 (2020), 101141.
[63] A.K. Adepu, S. Goskula, S. Chirra, S. Siliveri, S.R. Gujjula, V. Narayanan, Synthesis of a high-surface-area V2O5/TiO2–SiO2 catalyst and its application in the visible light photocatalytic degradation of methylene blue, RSC Adv. 9 (42) (2019) 24368–24376.
[64] M. Jiang, X. Cao, D. Zhu, Y. Duan, J. Zhang, Hierarchically porous N-doped carbon derived from ZIF-8 nanocomposites for electrochemical applications, Electrochim. Acta 196 (2016) 699–707.
[65] M. Chin, C. Cisneros, S.M. Araiza, K.M. Vargas, K.M. Ishihara, F. Tian, Rhodamine B degradation by nanosized zeolitic imidazolate framework-8 (ZIF-8), RSC Adv. 8 (47) (2018) 26987–26997.
[66] J. Bedia, V. Muelas-Ramos, M. Peñas-Garzón, A. Gómez-Avilés, J.J. Rodríguez, C. Belver, A review on the synthesis and characterization of metal organic frameworks for photocatalytic water purification, Catalysts 9 (1) (2019) 52.
[67] M. Ma, W. Guo, Z. Yang, S. Huang, G. Wang, Preparation and photocatalytic activity of TiO2/Fine char for removal of rhodamine B, . 2015 (2015) 1–5.